



Coherence-Enhanced Imaging of a Degenerate Bose-Einstein Gas

L. E. Sadler, J. M. Higbie, S. R. Leslie, M. Vengalattore, and D. M. Stamper-Kurn

Department of Physics, University of California, Berkeley, California 94720, USA

(Received 31 August 2006; published 12 March 2007)

We present coherence-enhanced imaging, an *in situ* technique that uses Raman superradiance to probe the spatial coherence of an ultracold gas. Applying this technique, we identify the coherent portion of an inhomogeneous degenerate ^{87}Rb gas and obtain a spatially resolved measurement of the first-order spatial correlation function. We find that the decay of spin gratings is enhanced in high density regions of a Bose-Einstein condensate, and ascribe the enhancement to collective atom-atom scattering. Further, we directly observe spatial inhomogeneities that arise generally in the course of extended-sample superradiance.

DOI: [10.1103/PhysRevLett.98.110401](https://doi.org/10.1103/PhysRevLett.98.110401)

PACS numbers: 03.75.-b, 42.50.Ct, 42.50.Gy

Ultracold Bose and Fermi gases present new possibilities for studying the conditions for and onset of macroscopic quantum coherence in condensed-matter systems, particularly under nonequilibrium conditions initiated by rapid changes of system parameters. A direct probe of coherence in these gases is essential to fully exploit this opportunity.

Limitations of existing techniques for measuring coherence in atomic gases have narrowed the scope of prior studies. Time-of-flight methods, in which coherence is detected through matter-wave interference, provide poor spatial resolution. This precludes detailed studies of coherence in inhomogeneous systems such as the borders of Mott-insulating regions of bosons in optical lattices [1], gases in disordered potentials [2], or systems undergoing a rapid [3–5] or first-order phase transition [6–9] to a superfluid state. A second technique, the imaging of irrotational flow as a signal for phase coherence, requires the system to be strongly agitated over extended periods of time. This perturbation prevents direct measurements of phase coherence in rapidly evolving systems or those near a phase transition.

In this Letter, we describe coherence-enhanced imaging, which allows the coherent portions of a gaseous system to be directly identified with high spatial resolution. Previous *in situ* imaging methods [10–12], being sensitive to the linear optical susceptibility of the trapped gas, allow the identification of the coherent portion of the gas only through its high optical density. In contrast, our imaging method relies on a nonlinear optical effect, superradiance-enhanced absorption, to gain access to the difference in coherence between portions of the gas.

We present two main results derived from coherence-enhanced images. First, we quantify coherence properties in a degenerate ^{87}Rb gas. Specifically, we directly map the coherent portion of a trapped Bose gas, obtaining spatially resolved measures of the condensate number and of the first-order spatial correlation function. Second, we perform the first spatially resolved study of extended-sample superradiance, revealing inhomogeneous collective scattering across the gas.

Collective light scattering can be regarded as a form of extended-sample superradiance [13–17] where pump light illuminating the sample places all scatterers into an excited state whence they optically decay. Considering specifically a gaseous atomic sample, such light scattering produces atoms that recoil with momentum $\hbar\mathbf{q} = \hbar\mathbf{k}_i - \hbar\mathbf{k}_s$, which is the difference between the momenta of the incident and scattered photons. In the case of Rayleigh superradiance, spatial coherence between the recoiling and stationary atoms creates a periodic density grating through matter-wave interference. This grating acts as a partially reflective mirror, oriented so as to scatter light in the same direction as previously scattered light. The mechanism for Raman superradiance, which is used in this work, differs in that interference between recoiling and stationary atoms creates a spin-polarization rather than a number-density grating and in that recoiling atoms no longer scatter light [18,19]. In either case, for a prolate sample, the enhanced light scattering is directed predominately along the end-fire modes, i.e., along the long axis of the gas. In previous work, the narrowly directed emission of light and atoms from the sample served as the primary signal used to study superradiance. Here we focus on a different signature of superradiance, namely, the collectively enhanced absorption of the pump light. Imaging this light yields detailed spatial information on the radiating sample.

The collective enhancement of the optical scattering rate depends on the quality of the grating formed in the gas. In turn, properties of the grating depend on the competition between a position-dependent loss of grating coherence and the coherent amplification of the grating by stimulated emission. The loss of grating coherence can occur due to Doppler broadening or collisional dephasing and loss. Considering just Doppler effects, a freely-propagating polarization grating decays after a correlation time $\tau_c \sim (q\Delta v)^{-1}$, which is the time it takes atoms propagating at momentum $\hbar\mathbf{q}$ to travel beyond the coherence length $\lambda = \hbar/m\Delta v$, with $(\Delta v)^2$ being the local atomic velocity variance and m the atomic mass. Thus, polarization gratings in gases with long coherence lengths, such as a Bose-Einstein condensate (BEC), persist much longer than those in non-

degenerate gases with short, temperature (T) dependent coherence lengths $\lambda_{dB} = \sqrt{2\pi\hbar^2/mk_B T}$. We note that the coherence length λ , which pertains to the first-order spatial correlation function of the matter-wave field, is related conventionally to the local velocity distribution via Fourier transforms [20,21].

In our experiment, we induce superradiance in a gas using multiple short pulses of light separated by a variable delay time τ . Thus, collective scattering is built up over multiple pulses only in the portion of the gas with $\tau \ll \tau_c$, while Doppler dephasing in the portion of the sample with $\tau \geq \tau_c$ suppresses the pulse-to-pulse growth of the polarization grating.

Our experiments were performed on prolate gases of ^{87}Rb in the $|F = 1, m_F = -1\rangle$ hyperfine state, held in a Ioffe-Pritchard magnetic trap with trap frequencies of $\omega_{x,y,z} = 2\pi(48, 48, 5) \text{ s}^{-1}$ in the transverse (\hat{x}, \hat{y}) and axial (\hat{z}) directions. The gas temperature was varied by the final settings used in rf evaporative cooling, yielding gases of 15×10^6 atoms at the Bose-Einstein condensation transition temperature of $T_c = 250 \text{ nK}$, and pure condensates of up to 1.6×10^6 atoms.

The light used for superradiance-enhanced imaging was directed along the \hat{y} axis, linearly polarized perpendicular to the \hat{z} magnetic field axis (Fig. 1), and detuned by 102 MHz above the $F = 1 \rightarrow F' = 1$ D1 transition ($k_i = 2\pi/795 \text{ nm}$). This detuning and polarization was chosen for two reasons. First, Rayleigh scattering is eliminated due to destructive interference among the transitions to the $F' = 1$ and the $F' = 2$ excited hyperfine states. This eliminates the dispersive phase shift that would otherwise cause aberrations in imaging the $\sim 10 \mu\text{m}$ wide cloud. Second, at this detuning, Raman superradiance occurs with highest gain to the $|F = 2, m_F = 1\rangle$ state; time-of-flight analysis

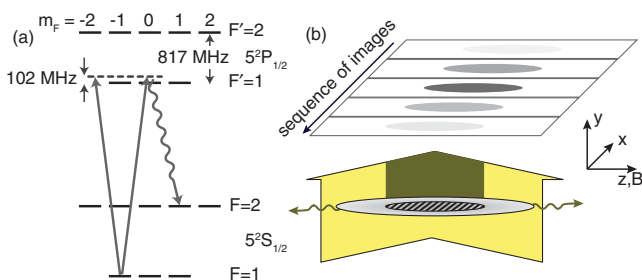


FIG. 1 (color). Experimental scheme for coherence-enhanced imaging. (a) Linearly polarized (along \hat{x}) imaging light, detuned 102 MHz above the $F = 1 \rightarrow F' = 1$ D1 transition, induces Raman superradiance at highest gain from the $|F = 1, m_F = -1\rangle$ initial state to the $|F = 2, m_F = 1\rangle$ final state. Zeeman sublevels are indicated, quantized along the magnetic field (\hat{z}) direction. (b) Such superradiance establishes a coherent polarization grating in spatially coherent portions of the gas, causing collective absorption of probe light and its reemission along the end-fire modes. Each incident pulse is imaged separately.

confirmed that gases were superradiantly pumped exclusively to this final state. This state possesses a nearly equal magnetic moment to the initial state, and the relative s -wave scattering lengths among all trapped states are nearly identical. As a result, effects on collective light scattering from both Zeeman and mean-field interaction shifts are made negligible.

Coherence-enhanced images of a pure condensate taken at this detuning demonstrate the spatial and temporal resolution of our technique (Fig. 2(b)). For these images, a BEC of 1.6×10^6 atoms was illuminated by a series of 100 μs -long pulses of light, with a $\tau = 68 \mu\text{s}$ delay between pulses. The transmitted part of each probe pulse was separately imaged at a diffraction-limited resolution of $\sim 6 \mu\text{m}$. The absorption by the condensate increases over several probe pulses due to collective Raman scattering. After achieving a maximum of 15%, the absorption diminishes as a large fraction of the condensed atoms have been optically pumped to the $|F = 2, m_F = 1\rangle$ state in which they no longer absorb probe light.

To estimate the maximum absorption expected for this sample, let us consider superradiant scattering solely into one end-fire mode and into one final atomic state ($|F = 2, m = 1\rangle$). In the case when half the atoms have been scattered and assuming simultaneous collective behavior by all atoms in the sample, the optical depth is enhanced by a factor $\mathcal{E} = \frac{R_j}{R_{\text{tot}}} \frac{f_j}{4} N_0 A_\Omega$. Here, $R_j/R_{\text{tot}} = 0.28$ is the branching ratio for scattering into the preferred final state $|j\rangle$, f_j is an angular term that includes the dipole emission pattern, N_0 is the total atom number, and A_Ω is a phase-matching factor [16]; here $N_0 A_\Omega = 5800$. We thus predict a maximum enhancement factor $\mathcal{E} \approx 60$, somewhat greater than the observed $\mathcal{E} \approx 10$.

The discrepancy between the expected and observed absorption is not surprising given the significant spatial

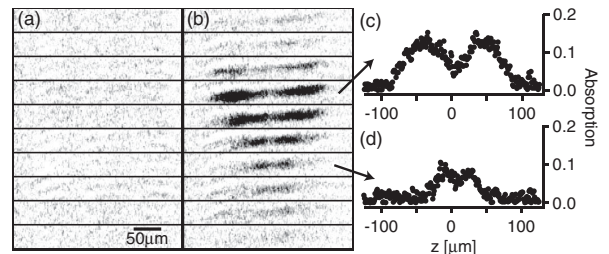


FIG. 2. *In situ* imaging of coherence in a trapped Bose gas. Coherence-enhanced absorption images are shown for single gaseous samples at (a) $T/T_c = 1.3$ and (b) $T/T_c = 0.3$. Each of ten frames, shown in temporal order from top to bottom, is illuminated by a 100 μs pulse of light followed by a $\tau = 68 \mu\text{s}$ delay. Doppler dephasing during the delay times suppresses superradiance except in coherent portions of the gas. Thus, enhanced absorption is seen only in the condensed portions of the degenerate sample. As shown in (c) and (d), the absorption signal varies across the cloud with collective enhancement occurring first at the ends of the extended sample.

features seen in the coherence-enhanced images (Fig. 2), where the ends of the extended sample darken earlier than the denser cloud center. Thus, the maximal enhancement of light scattering does not occur simultaneously throughout the cloud, diminishing the overall enhancement of absorption as compared with our estimate.

Models of superradiance have been proposed that predict the spatial inhomogeneities that we observe [22,23]. In these models, the initiation of collective scattering is treated as in Dicke's original work [13] with light scattering leading to the occupation of atomic recoil modes that are propagating replicas of the unscattered atomic state. Once collective scattering dominates, a semiclassical picture emerges in which light propagating down the long axis of the sample acquires its highest intensity at the tip of the gas. Atoms located there are more strongly stimulated by the field and scatter light earlier than those in the center of the cloud. While the development of spatial structure was indicated indirectly by previous studies [18,21], coherence-enhanced imaging gives unprecedented temporal and spatial resolution of the entire superradiance process.

Beyond providing insight on the dynamics of superradiance, these multiple-frame images yield quantitative information about spatial coherence in trapped gases. For

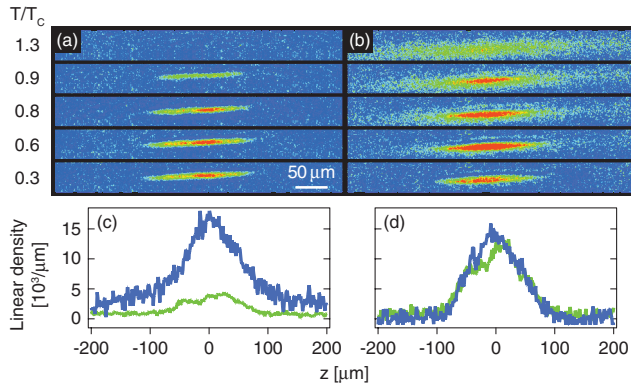


FIG. 3 (color). Spatial maps of the condensate. (a) Coherence-enhanced images are used to map the net coherence-enhanced absorption (total number of missing probe photons summed over all image frames). Here, superradiant emission was completed in four probe pulses, i.e., within $\sim 600 \mu\text{s}$, shorter than the correlation time τ_c in the condensate (see Fig. 4). The remaining image frames are used to determine the incident probe fluence and to eliminate the slight linear absorption signal from the noncondensed atoms. (b) Off-resonant linear Raman absorption images reveal the combined densities of the condensed and normal fractions of the gas. Linear-density distributions (summed across \hat{x}) of the total number (blue), from linear absorption imaging, and of the condensate number (green), from coherence-enhanced imaging, are shown for (c) a gas with small condensate fraction ($T = 250 \text{ nK} = 0.9T_c$) and (d) for a nearly pure condensate at $T = 30 \text{ nK} = 0.3T_c$. The coherence-enhanced images indicate condensate numbers of 7×10^5 and 1.4×10^6 in (c) and (d), respectively.

example, in contrast with linear absorption imaging, coherence-enhanced imaging allows the coherent fraction of the partially condensed Bose gas to be identified directly. Images obtained by each of these methods are compared in Fig. 3. The off-resonant linear absorption images, taken with light 200 MHz below the D2 $F = 1 \rightarrow F' = 2$ transition to eliminate dispersive phase shifts, show a typical progression of density distributions from Gaussian for $T/T_c > 1$, to bimodal, and finally, to a single parabolic (condensate) density distribution for the smallest T/T_c . In contrast, coherence-enhanced imaging selectively resolves the condensed portion of the gas, present at $T/T_c < 1$. This selectivity stems from our choosing a gap time $\tau = 68 \mu\text{s}$ that is longer than the correlation time for the thermal component ($\tau_c = 50 \mu\text{s}$ at a typical temperature of 200 nK), but much shorter than the Doppler coherence time of the condensate (Fig. 4).

Under the assumption that the condensate is completely optically pumped to the $|F = 2, m_F = 1\rangle$ state during multiple-pulse superradiance, our assessment of the total number of absorbed photons in a coherence-enhanced imaging sequence directly quantifies the condensate number. This assumption is supported by time-of-flight studies of Raman superradiance [18,19]. However, our data in Figs. 3(c) and 3(d) do suggest that the condensate's population is undercounted at its center.

By varying the delay times τ in our imaging sequence, we may also use coherence-enhanced imaging to obtain a spatially resolved measurement of the first-order spatial correlation function. For this purpose, we determine, at each pixel location, the ratio of absorption between the first and second frame in the image. The optical absorption signal in the second frame quantifies the modulation depth of interference at each location between the remaining stationary gas and its replica, displaced by $\delta r = \hbar q \tau / m$. The absorption ratio is large in portions of the gas with high spatial coherence and tends to unity when δr exceeds the local coherence length [21].

Multiple-pulse coherence-enhanced images were taken of identically prepared gaseous samples with variable de-

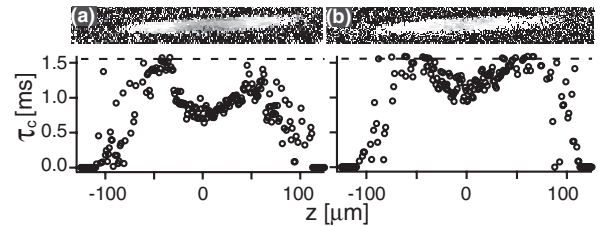


FIG. 4. Maps of correlation times τ_c (see text for definition) shown for degenerate Bose gases at (a) $T/T_c = 0.3$ and (b) $T/T_c = 0.8$. Longitudinal cross sections are shown below the corresponding images. The Doppler limit on τ_c (dashed line) matches the measurement at tips of the condensate. The reduction of τ_c at the condensate center is ascribed to nonlinear atom-atom elastic scattering. Gray scale runs from 0 to 1.6 ms.

lay times τ . In Fig. 4 we present maps of the characteristic correlation time $\tau_c(x, z)$, which we obtain at each pixel as the $1/e$ decay time as determined by Gaussian fits of the absorption ratio versus delay time. We observe a maximal correlation time, $\tau_c = 1.6$ ms, that is consistent with the time required for recoiling atoms to travel through the condensate. This confirms that BECs are coherent across their radial width [24–27].

Surprisingly, however, we find that τ_c diminishes in the center of the BEC, most dramatically for samples at the lowest temperatures at which the condensate fraction and density are the highest. We ascribe the lowering of τ_c to nonlinear collisional depletion of the propagating spin grating formed in superradiance [28]. The linear (noncollective) per particle scattering rate of atoms recoiling at $v = \hbar q/m$ propagating through the stationary portion of the gas, $\Gamma_l = n\sigma v = 300 \text{ s}^{-1}$, with σ being the total collision cross section, is too small to significantly affect the observed correlation times. However, in a coherent gas, such scattering is enhanced to the extent that the total number of collisions exceeds the number of quantum states available to the collision products. We estimate the enhanced nonlinear scattering rate in a volume with a radius that is equal to the distance the sample recoils before the grating decays to be $\Gamma_{nl} = \sqrt{\hbar^2 \sigma n n_s} / (6\pi m^2) \simeq 1/(500 \mu\text{s})$, where n_s is the density of the scattered atoms. This rate agrees with the observed coherence decay rates at the center of the condensate. In more dilute regions, such as the tips of the condensate or in the less dense condensate formed at higher temperatures, the collective enhancement of collisional losses is weaker, and, thus, higher values of τ_c are observed. We note that these collisional losses can be suppressed by exciting fewer atoms to the $|F = 2\rangle$ state or by exciting them to recoil velocities below the local speed of sound [28] allowing for measurements of the coherence length in dense condensates.

As we have shown, coherence-enhanced imaging yields simultaneous information both on the spatial coherence of an ultracold gas and also on superradiance in extended samples. However, the spatial inhomogeneities formed during superradiance are an inconvenient feature that complicates our analysis. Alternatively, one could employ a two-photon stimulated Raman transition to set up a uniform initial polarization grating, and then image the collectively enhanced absorption of a subsequent single probe beam. Such an approach is technically complicated by the

need for setting a precise frequency difference between two laser beams and also by sensitivity to overall Doppler shifts for a possibly moving gas sample. Our method avoids such complications.

On the other hand, coherence-enhanced imaging as implemented here has allowed for the first direct study of the onset of inhomogeneous collective scattering. In future studies, fluctuating asymmetries in the spatial structures that develop spontaneously during superradiance may be used to characterize further the quantum fluctuations that play a role in its early stages [23].

We thank P. Meystre, H. Uys, and D. Schneble for discussions and comments. This work was supported by the NSF and the David and Lucile Packard Foundation. S. R. L. acknowledges support from the NSERC.

-
- [1] D. Jaksch *et al.*, Phys. Rev. Lett. **81**, 3108 (1998).
 - [2] J. E. Lye *et al.*, Phys. Rev. Lett. **95**, 070401 (2005).
 - [3] W. H. Zurek *et al.*, Phys. Rev. Lett. **95**, 105701 (2005).
 - [4] T. W. B. Kibble, J. Phys. A **9**, 1387 (1976).
 - [5] W. H. Zurek, Nature (London) **317**, 505 (1985).
 - [6] E. Altman *et al.*, New J. Phys. **5**, 113 (2003).
 - [7] K. Krutitsky and R. Graham, Phys. Rev. A **70**, 063610 (2004).
 - [8] A. Kuklov *et al.*, Phys. Rev. Lett. **93**, 230402 (2004).
 - [9] T. Kimura *et al.*, Phys. Rev. Lett. **94**, 110403 (2005).
 - [10] M. Andrews *et al.*, Science **273**, 84 (1996).
 - [11] M. Andrews *et al.*, Phys. Rev. Lett. **79**, 553 (1997).
 - [12] L. Hau *et al.*, Phys. Rev. A **58**, R54 (1998).
 - [13] R. H. Dicke, Phys. Rev. **93**, 99 (1954).
 - [14] N. Skribanowitz *et al.*, Phys. Rev. Lett. **30**, 309 (1973).
 - [15] R. Florian *et al.*, Phys. Rev. A **29**, 2709 (1984).
 - [16] S. Inouye *et al.*, Science **285**, 571 (1999).
 - [17] M. Dreher *et al.*, Phys. Rev. Lett. **93**, 095001 (2004).
 - [18] D. Schneble *et al.*, Phys. Rev. A **69**, 041601(R) (2004).
 - [19] Y. Yoshikawa *et al.*, Phys. Rev. A **69**, 041603(R) (2004).
 - [20] F. Zambelli *et al.*, Phys. Rev. A **61**, 063608 (2000).
 - [21] Y. Yoshikawa *et al.*, Phys. Rev. Lett. **94**, 083602 (2005).
 - [22] J. C. MacGillivray and M. S. Feld, Phys. Rev. A **14**, 1169 (1976).
 - [23] H. Uys and P. Meystre, cond-mat/0602343 [Phys. Rev. A (to be published)].
 - [24] M. R. Andrews *et al.*, Science **275**, 637 (1997).
 - [25] J. Stenger *et al.*, Phys. Rev. Lett. **82**, 4569 (1999).
 - [26] E. Hagley *et al.*, Phys. Rev. Lett. **83**, 3112 (1999).
 - [27] I. Bloch *et al.*, Nature (London) **403**, 166 (2000).
 - [28] A. Chikkatur *et al.*, Phys. Rev. Lett. **85**, 483 (2000).